crystals

MDPI

Article

In Situ Observation of Epitaxial Growth during Evaporative Simultaneous Crystallization from Aqueous Electrolytes in Droplets

Frederico M. Penha [1,2,*], Fábio R. D. Andrade [3], Amanda S. Lanzotti [2], Paulo F. Moreira Junior [2], Gustavo P. Zago [2] and Marcelo M. Seckler [2]

[1] Division of Resource Recovery, Department of Chemical Engineering, KTH Royal Institute of Technology, 114 28 Stockholm, Sweden
[2] Department of Chemical Engineering, Polytechnic School, University of São Paulo, São Paulo 3550308, Brazil; amandaa.slanzotti@gmail.com (A.S.L.); pfmoreir@gmail.com (P.F.M.J.); gustavo.zago89@gmail.com (G.P.Z.); marcelo.seckler@usp.br (M.M.S.)
[3] Geosciences Institute, University of São Paulo, São Paulo 3550308, Brazil; dias@usp.br
* Correspondence: fremp@kth.se

Abstract: In this study, crystallization phenomena were investigated by real-time in situ observation of seeded droplets under evaporation using a self-developed hot-stage platform. Ternary solutions at eutonic conditions at 25 °C were investigated for the following systems: NaCl–KCl–H_2O, NaCl–$CaSO_4$–H_2O, and NaCl–Na_2SO_4–H_2O. Evidence of epitaxial growth was found for aqueous NaCl–KCl and aqueous NaCl–Na_2SO_4. Sodium chloride nucleated and grew epitaxially upon the other substrates in a larger proportion compared with the inverse. This observation could be related to the higher solubility, and consequently higher residual supersaturation of NaCl regarding the other components. Hopper-like NaCl crystals developed in almost all systems. The results may help devise strategies to control particle morphologies and purity in industrial crystallization from complex systems.

Keywords: simultaneous crystallization; epitaxial particles; real-time monitoring; crystallization from ternary solutions

Citation: Penha, F.M.; Andrade, F.R.D.; Lanzotti, A.S.; Moreira Junior, P.F.; Zago, G.P.; Seckler, M.M. In Situ Observation of Epitaxial Growth during Evaporative Simultaneous Crystallization from Aqueous Electrolytes in Droplets. *Crystals* **2021**, *11*, 1122. https://doi.org/10.3390/cryst11091122

Academic Editor: Borislav Angelov

Received: 18 August 2021
Accepted: 10 September 2021
Published: 15 September 2021

1. Introduction

Crystallization processes are well established for the production of a wide range of particulate products as well as for purification and separation processes [1]. They are usually designed to obtain a single solid compound and involves several simultaneous processes, e.g., heat transfer, nucleation, crystal growth and dissolution [2]. For applications such as water reuse, it is necessary to promote the concomitant formation of several crystalline compounds. Simultaneous crystallization of more than one solute tends to yield crystals with irregular sizes and shapes [3] that retain solution and, therefore, form solid precipitates with high moisture. The end products of such crystallizers may consist of mono- and poly-crystalline particles of single compounds or polycrystalline particles of mixed composition.

Our previous studies on batch evaporative simultaneous crystallization have shown that epitaxial growth is an important phenomenon affecting the morphology and composition of the crystals in the NaCl–KCl–H_2O system, while it was not observed in the NaCl–$CaSO_4$–H_2O system [4–7]. Although advances have been made, there are still several open questions regarding the epitaxial growth in eutonic systems in industrial crystallizers, such as the possible relations between epitaxy and growth conditions. Given the extensive application of epitaxial growth in conductive and semi conductive materials [8,9], the available literature focuses mainly on the growth of epitaxial monolayers or thin films. Epitaxial growth of thin layers commonly uses molecular beam epitaxy, chemical vapor

deposition or liquid-phase epitaxy, under high temperatures and high vacuum [10]. Few studies address epitaxial growth in conventional systems of industrial crystallization.

The classical definition of epitaxy refers to the structural similarity at the interface of growing crystals, in terms of interatomic distances, the nature of the atoms or atomic groups and chemical bonds [11–13]. Epitaxy is a particular case of heterogeneous nucleation, that usually results in oriented growth of the nuclei on the substrate [14–16], according to the more coherent crystallographic direction. Epitaxial growth of ionic crystals was experimentally evaluated by Royer [17] apud Markov [12], who concluded that for heteroepitaxy to occur—where the nucleating crystal and the substrate have different composition—the crystalline planes in contact must have similar symmetry and chemical bonds, and that the difference between lattice parameters of the two solids may not exceed 15%. Epitaxial nucleation may lead to structural modifications in thin films at early stages of crystallization, so that the crystalline structure of the nucleating phase is altered to match the substrate [18–20].

Epitaxial growth via 2D lattice matching can be mathematically estimated using the method by Hillier and Ward [21], based on a rationale that epitaxial growth takes place if the crystal structures of the substrate and the nucleating phase match in a given azimuthal angle. Geometric fitting between substrate and deposit differs from conventional potential energy calculation, that rely on optimizing the interaction energy of the substrate-deposit atom over various azimuthal angles [22]. In short, the dimensionless potential energy can be calculated at the substrate-deposit interface associated with a characteristic lattice match. Mathematically, the calculation matches the substrate and deposit lattice vectors (a1, a2, α for substrate and b1, b2, β for the overlayer) over a range of azimuthal angle (μ) between them, according to Equation (1).

$$\frac{V}{V_0} = 1 - \frac{1}{2MN} \times \frac{\sin(M\pi p_x)\sin(N\pi q_x)}{\sin(\pi p_x)\sin(\pi q_x)} - \frac{1}{2MN} \times \frac{\sin(M\pi q_y)\sin(N\pi p_y)}{\sin(\pi q_y)\sin(\pi p_y)} \quad (1)$$

where p_x, p_y, q_x, q_y are parameters that relate lattice vectors of substrate and deposit and M, N are the number of deposit lattices along two dimensions. The global minimum of V/V_0 at an azimuthal angle can be used to infer the epitaxial relation. Three types of 2D lattice matching can be observed and correlated with the dimensionless potential energy (V/V_0): (i) commensurism, where the lattice sites of the substrate and deposit fully overlap each other—$V/V_0 \approx 0$; (ii) coincidence, where the lattices of the deposit overlaps on a certain lattice vector of the substrate, but not all—$V/V_0 \approx 0.5$; and (iii) incommensurism, where no overlap between the lattices of the substrate and deposit are seen—$V/V_0 \approx 1$.

Epitaxial growth can result in oriented crystals on the substrate, a condition favored by similar molar volumes between both substances [6]. The mutual orientation between crystals is also influenced by temperature, supersaturation and imperfections in the substrate [11,12]. The growth mechanism may be described considering the free energy at the interface. If the sum of the surface energy of the epitaxial layer and the interfacial energy between the crystals is less than or equal to the energy of the substrate surface ($\gamma_E + \gamma_i \leq \gamma_s$), then the preferred mechanism will be layer-by-layer growth, which means that a full layer is grown before the subsequent one. For smaller differences between the lattice parameters, the interfacial energy will also be low, accounting for the stronger tendency among these crystals to form monolayers. In general, the two crystal planes with the highest structural coherence tend to align parallel to each other [23,24]. In cases of high epitaxial fit between phases with very similar lattice constants, the nucleating phase tends to grow as a thin film on the substrate, covering its entire surface [25,26], in a process known as Frank van der Merwe growth mechanism. For higher lattice mismatch, two processes are envisaged, the Stranski–Krastanov and the Volmer–Weber mechanisms. The Stranski–Krastanov mechanism starts with the nucleation of a thin layer of a stressed structure that, beyond a critical thickness, is followed by 3D crystal-islands [27]. In this case, the sum of the energy of the epitaxial layer and the energy of the interface between the crystals is larger than the surface energy of the substrate ($\gamma_E + \gamma_i > \gamma_s$), and three-

dimensional nuclei are preferentially formed. If the interface energy between crystals is even larger, the Volmer–Weber mechanism prevails, in which 3D nuclei are formed directly on the substrate crystal [28]. The formation of 3D nuclei also relies on a suitably high ionic diffusion coefficient for their migration and deposition onto the substrate surface [29].

In the present contribution, epitaxial growth is analyzed in the context of crystallization for desalination of industrial wastewater, water reuse and dissolved salts recovery. Industrial wastewaters are multicomponent solutions, containing salts of various solubilities. Experiments of seeded evaporative crystallization from pairs of solutes under eutonic conditions at 25 °C were carried out and monitored by in situ microscopic observations. The ternary systems (NaCl–KCl–H_2O), (NaCl–$CaSO_4$–H_2O) and (NaCl–Na_2SO_4–H_2O) were chosen because they are prevalent in several industrial aqueous effluents [30]. This contribution aims to improve the understanding of crystallization phenomena in multicomponent systems, consequently enhancing efficiency of downstream processes of water and solute recovery.

2. Materials and Methods

2.1. Eutonic Conditions

Phase diagrams for the studied ternary systems at 25 °C were calculated with the thermodynamic modelling software OLI Studio 9.6 (OLI Systems, Inc., Parsippany, NJ, USA, Figure 1).

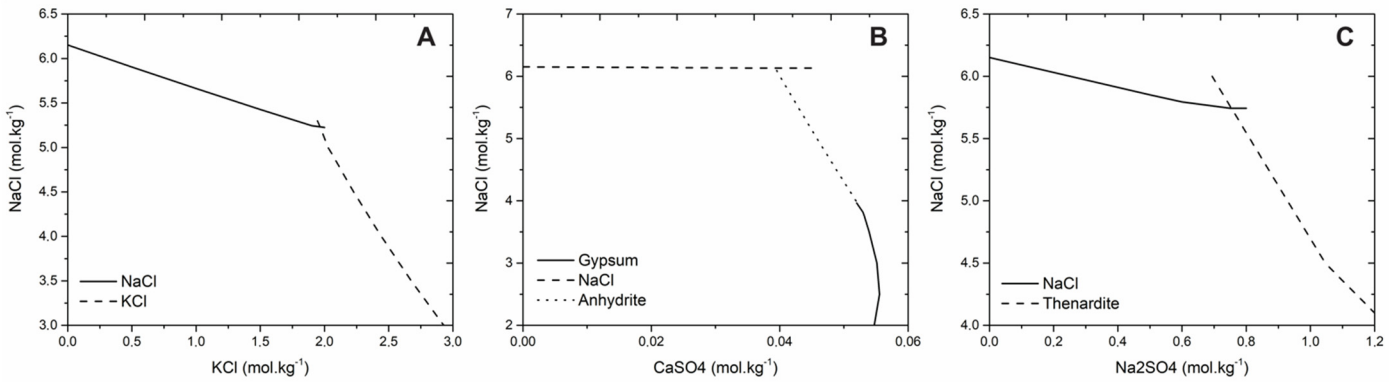

Figure 1. Phase diagrams for the aqueous ternary system at 25 °C: (**A**) NaCl–KCl; (**B**) NaCl–$CaSO_4$; and (**C**) NaCl–Na_2SO_4.

The three systems have eutonic points—where the two solubility lines meet—and the respective solid phases and solution are in equilibrium. The eutonic concentration for each system is shown in Table 1.

Table 1. Eutonic concentrations of the studied systems at 25 °C.

System	(Salt 1) (mol·kg_{water}^{-1})	(Salt 2) (mol·kg_{water}^{-1})
NaCl $_{(1)}$ + KCl $_{(2)}$	5.24	1.95
NaCl $_{(1)}$ + $CaSO_4$ $_{(2)}$	6.10	0.04
NaCl $_{(1)}$ + Na_2SO_4 $_{(2)}$	5.74	0.74

2.2. Experimental Solutions

$CaCl_2$ (CAS 10035-04-8), KCl (CAS 7447-40-7), NaCl (CAS 7647-14-5) and Na_2SO_4 (CAS 7757-82-6) analytical grade reagents (LabSynth, Diadema, São Paulo, Brazil—P.A.—A.C.S, purity > 99.5%) and distilled water were used to prepare solutions for each experiment. Solutions were prepared in concentrations near the eutonic point, but slightly undersaturated by adding 2.5 wt% extra water. The minor undersaturation avoids the nucleation during the preparation of the experiment and promotes a slight dissolution of the seeds, removing solids adhered to the seed crystals and correcting irregularities on their surfaces.

The salts and distilled water were weighed and mixed in an Erlenmeyer covered with a lid. The suspension was placed in a heating plate at 50 °C with magnetic stirring, to ensure full dissolution. The salts were directly weighed for all the systems except for ($NaCl–CaSO_4–H_2O$). As the dissolution of $CaSO_4$ is extremely slow, the required amount of Ca^{2+} and SO_4^- ions were obtained by dissolving $CaCl_2$ and Na_2SO_4. The added Na^+ and Cl^- ions were subtracted from the necessary amount of NaCl to be added. Around 50 mL of each solution was prepared and stored hermetically closed. Before performing the experiments, solutions were pre-heated to 25 °C.

2.3. Seeds Selection

Seed crystals of NaCl, KCl and Na_2SO_4 were taken from their respective commercial reagent (analytical grade) to provide comparability with an industrial seeding scenario. Every compound was used as seed in their respective systems: NaCl and KCl seeds were used in the ($NaCl–KCl–H_2O$) system; NaCl and Na_2SO_4 seeds were used in the ($NaCl–Na_2SO_4–H_2O$) system; and NaCl was used as seed in the ($NaCl–CaSO_4–H_2O$) system. Experiments were not performed using $CaSO_4$ seeds as the commercial reagent characteristic particle sizes ($\ll$50 μm) hampered the seed selection. Moreover, discrepant characteristic sizes among $CaSO_4$ and all the other salts investigated made the concomitant visualization of such pair of salts on the optical microscope impossible.

The seeds were first classified into the size range of interest—between 500–1000 μm—through sieving the salts in a magnetic vibrating platform for about 45 min. SEM images of the seed crystals are shown in Figure 2. Seeds were manually selected under a stereomicroscope (Nikon SMZ800N, Nikon Instruments Inc., Tokyo, Japan) avoiding seriously damaged or broken crystals.

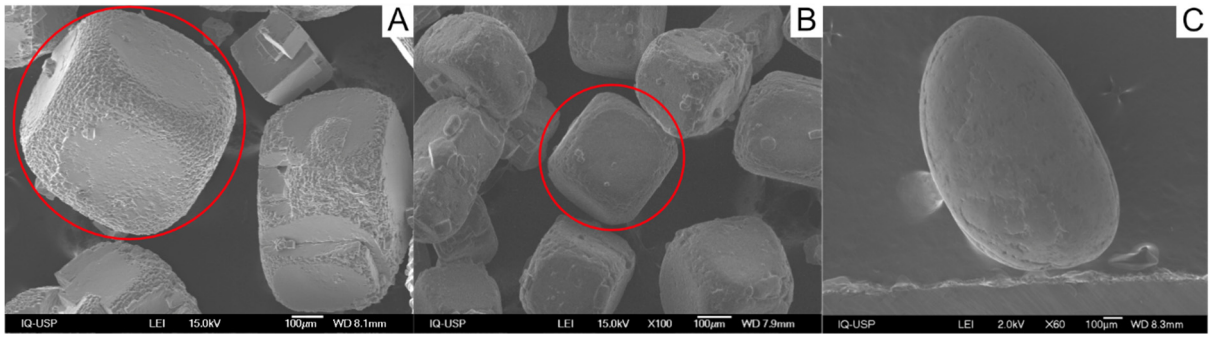

Figure 2. Sample SEM images of typical morphologies of crystals of (**A**) NaCl, (**B**) KCl, and (**C**) Na_2SO_4 from the commercial reagents.

2.4. Hot Stage Device

A hot stage for optical microscopy was built using a stainless-steel heat exchanger coupled to an aluminum plate with a hole or window (Ø = 5 mm) to allow transmission of light (Figure 3). The heat exchanger was connected to a thermostatic bath (Lauda Eco RE 620, Lauda China Co., Ltd., Nanjing, China) for temperature control. A modified microscopy slide, comprised by a glass ring attached to a glass plate, was placed on the aluminum plate with the sample holder aligned with the hole (window). This apparatus minimizes the influence of external factor, such as air convection, on the evaporation of the droplets of solution. The top of the glass ring containing the droplet remained open to enable solvent evaporation. The total volume of the crystallization chamber was 1.15 mL.

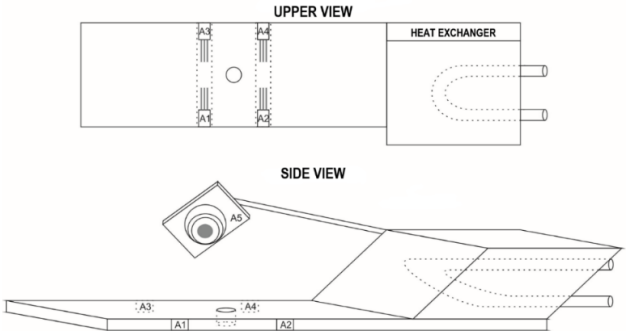

Figure 3. Schematic views of the hot-stage platform, where A1–A4 represent temperature sensors type LM35 and A5 represents the infrared thermometer type MLX90614.

Experiments were observed under an optical polarized light microscope (Olympus® BX60F-3, Olympus Microscopes, Shinjuku City, Tokyo, Japan). Temperature was monitored using a free hardware prototyping platform (Arduino Uno, ATmega 328P, Arduino LLC, Ivrea, Italy). Four analogue temperature sensors (LM35, Texas Instruments, Dallas, TX, USA) were symmetrically placed in gutters around the hole in the aluminum plate. These sensors require no calibration and provide precise temperature measurements (±0.25 °C) in the range of −55 to 150 °C. Additionally, an infrared (IR) thermometer (MLX90614, Melexis, Belgium) was attached to the hot stage, measuring temperature simultaneously in the sample and in the room with relatively high precision (±0.50 °C) in the range from −40 to 125 °C. An algorithm was written in C++ language to enable storage of the temperature data. The temperature was recorded every 3 s.

2.5. Static Droplet Evaporative Crystallizer

The experiments were designed to enable water evaporation from the solution due to the difference between the water vapor pressure in the saline solution and the water partial pressure in the air. Room temperature during the experiments was kept at 21 °C while the solution was maintained at 25 °C. Evaporation rates were measured using an analytical scale in parallel experiments in the same conditions. Value was found to be ~0.002 min^{-1} ($g_{evaporated\_water} \cdot g_{initial\_water}{}^{-1} \cdot min^{-1}$).

For each run, a 50 µL droplet of the saline solution at approximately 25 °C was placed on the crystallization chamber on the hot stage where temperature was kept constant at 25 °C. A single crystal seed was carefully immersed in the droplet and photomicrographed (MOTICAM 10 CMOS MP, Motic Group, Hong Kong, China) every minute for about 60 min.

At the end of each run, the crystals were carefully removed from the solution, washed with ethanol, and dried in an oven for approximately 1 h. Crystals were further analyzed using Scanning Electron Microscopy (SEM—JEOL JSM-7401F, Tokyo, Japan) coupled with an Energy Dispersive System (EDS).

3. Results and Discussion

3.1. NaCl–KCl–H_2O System

Images of the NaCl–KCl–H_2O system seeded with NaCl are displayed in Figure 4. The seed presents abundant fluid inclusions, noticeable as dark spots in the crystals [6]; it underwent slight dissolution at the beginning of the experiment, evidenced by a small decrease in size in the first minutes. After 10 min, the NaCl seed crystal started to grow, developing smooth surfaces, well-formed edges, and cubic habit. Around 20 min after the evaporation started, several individual crystals appeared in the droplet. This nucleation event is probably heterogeneous, triggered by factors such as nano-impurity particles in solution, phase boundaries [31] and local supersaturation spots. These new crystals developed hopper habits, indicated by the smooth square-ring on the border and fluid inclusions distribution, suggested by the dark spots in their center. The emergence of such crystals is unwanted, as they consume supersaturation and interfere with the epitaxial

phenomena around the seeded crystal. The control of the supersaturation, although desirable, is unfeasible in ternary solutions of highly soluble salts undergoing simultaneous crystallization. Simultaneous crystallization can only happen in the eutonic point, an invariant combination of the concentration of both salts, temperature, and pressure, with no degree of freedom. Highly soluble inorganic salts have very narrow metastable zones, leaving no room to adjust supersaturation levels. Hence, the slightest amount of water evaporation induces crystallization almost immediately and maintains the solution at the eutonic concentration [5]. For this reason, instead of controlling supersaturation, we turned our efforts to maintain the same evaporation rates in all experiments. By keeping constant evaporation rates and both compounds close to saturation levels, the residual supersaturation of each salt can be approximated as the driving force for its respective crystallization.

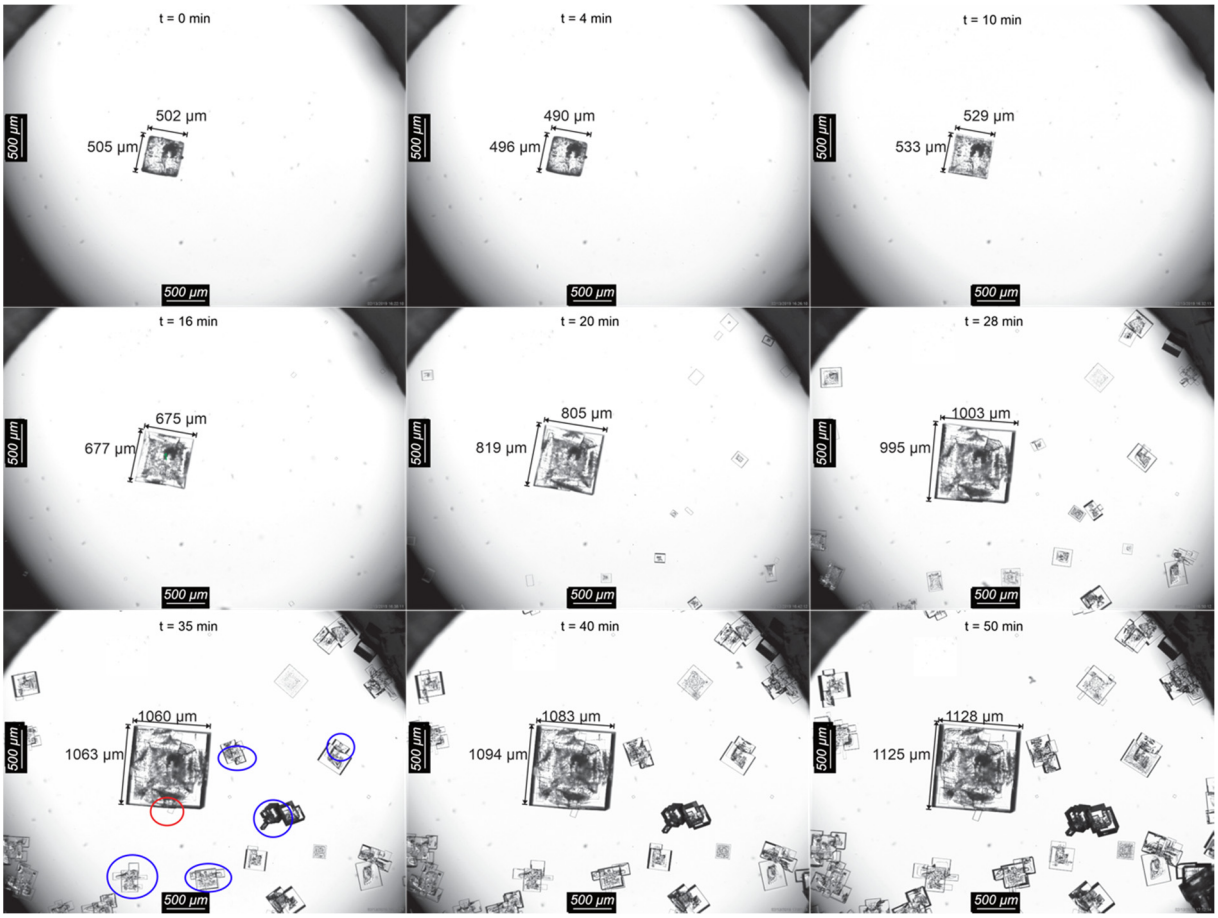

Figure 4. Optical photomicrographs along time of the NaCl–KCl–H_2O droplet under evaporation seeded with NaCl. A crystal growing on the surface of the seed is surrounded with the red circle at the frame t = 35 min. Blue circled crystals indicate other possible epitaxially grown crystals.

After circa 35 min, crystals can be seen on the surface of the crystals nucleated in solution (blue circles in Figure 4). It is unclear, however, whether these crystals can be evidence of epitaxial growth. As these crystals arise stochastically in the solution, it is also possible that nuclei from different salts formed both spatially and temporally close to one another, such that the polycrystalline sets circled in blue are simply agglomerates. Nuclei of different composition will have different growth rates, hence there will be a delay regarding the detection of those crystals, which can mislead our interpretation into characterizing them as epitaxy generated. Unfortunately, for the system NaCl–KCl–H_2O (Figure 4) it was not possible to identify the crystals composition directly through optical

microscopy. A closer look at those crystals using SEM was also not possible, as recognition and matching between optical microscopy and SEM images were not feasible.

NaCl seed surface grew free of foreign crystals until around 30 min of experiment, when a single crystal appeared at its surface (red circle in Figure 4). Both crystals continued to grow until the end of the experiment.

NaCl seed developed flat and smooth surfaces, usually associated with slow growth. This is surprising as hopper's growth, commonly associated to NaCl growth [32], was expected. The hopper habit is favored at high supersaturations [33,34], which is not consistent with the formation of smooth surfaces. To better understand this unexpected behavior, the growth of single NaCl crystal was observed in a NaCl-H_2O droplet solution saturated under the same conditions used in the ternary system experiments, in which the hopper habit can be promptly seen after a few minutes of evaporation (Figure S1). Thus, at eutonic concentrations of the ternary system NaCl–KCl–H_2O during evaporation NaCl growth resulted in smoother crystal surface.

Crystal growth is commonly divided into (i) diffusion of the growth units from the bulk solution to the crystal surface and (ii) integration of these units to the crystalline surface, and is influenced by factors such as temperature, solvent, supersaturation and by the ions and molecules presents in the surface layer. For relatively high soluble compounds, such as NaCl, the diffusion is usually the limiting step, as integration of the units to the crystal surface can be considered instantaneous. However, smooth growth is known to be surface integration-controlled [1]. Considering this scenario, a possible explanation for the development of smooth surfaces on the NaCl seed may be that the presence of the K^+ ions in the solution causes them to accumulate on the stagnant liquid layer around the growing crystal, and thus at the surface of the growing crystal. The presence of foreign ions might slow the incorporation of NaCl growth units to the NaCl-substrate crystal, forcing slower and more ordered growth, leading to smoother surfaces. It is important to highlight that, even though K^+ ions are present at the growing surface of NaCl crystals, the incorporation of these ions on the NaCl crystal lattice, also known as isomorphic substitution, is not expected under the temperature and pressure conditions in this work [35,36].

Optical microscopy images obtained in situ during crystallization of the ternary system NaCl–KCl–H_2O seeded with KCl are shown in Figure 5. During the first 12 min of crystallization, a slight dissolution of the seed crystal took place. Thereafter crystal growth healed the edges of the seed crystal. At 18 min, the surface started to develop roughness which became visibly new crystals at 22 min. After 26 min, crystals start growing on the surfaces of the KCl seed. These nucleation events are possibly epitaxial, visible in the photomicrographs and confirmed through EDS analysis. Between 35 and 42 min of crystallization, the crystals that were formed in opposite sides of the seed crystal surface (marked with a red circle in Figure 5) reached one another at the center of that surface and seemed to partially engulf the KCl seed.

SEM-EDS analysis of the NaCl seed grown in the ternary system is shown in Figure 6A. Its outer edges are well formed, and facetted epitaxial KCl crystals developed on the substrate. Some KCl crystals are aligned with the substrate crystal, some are not. The epitaxy generated KCl deposits have not partially engulfed the NaCl substrate surface, as have NaCl deposits upon the KCl substrate (Figure 6C). Besides, epitaxial nucleation and growth of KCl on NaCl is minor compared to epitaxy of NaCl on KCl seed. This may occur because the surface of the NaCl seed grew smooth, containing less kinks and steps that promote nucleation. Alternatively, it could be due to differences between the solubilities of NaCl and KCl. The KCl and NaCl crystals that were formed in solution away from the seed were also examined by SEM-EDS (Figure 6B), occurring both as single crystals and mixed polycrystals. Dust-like particles on the surface of the crystals arise due to drying of the reminiscent solution layer on top of the crystal, as reported elsewhere [5]. As KCl formation on the seed surface was not substantial, it is likely that upon evaporation the KCl supersaturation rose, so the initial burst of primary crystals in solution was probably from KCl. Yet, NaCl single particles,

which are not expected, are also visible in Figure 6B, most likely due to local supersaturation and primary heterogeneous nucleation.

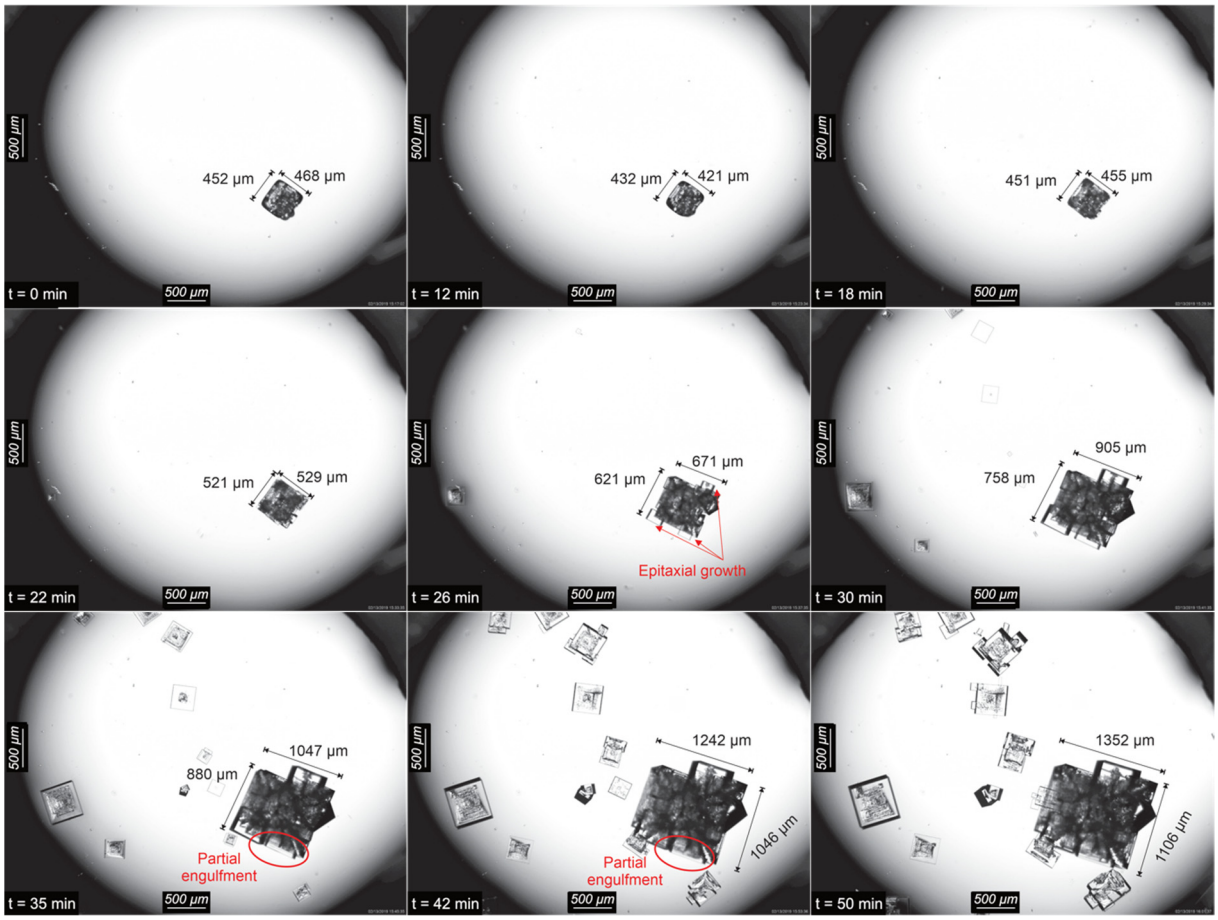

Figure 5. Optical photomicrographs of a NaCl–KCl–H_2O droplet seeded with KCl under evaporation.

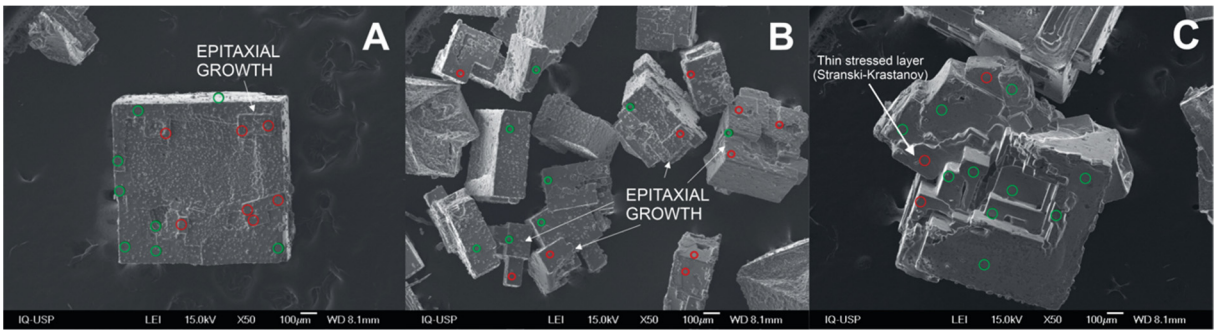

Figure 6. SEM image of: (**A**) NaCl seed grown, (**B**) crystals resulting from primary nucleation (not related to the seed) on the experiment seeded with NaCl, and (**C**) KCl seed grown after 60 min in the NaCl–KCl–H_2O droplet under evaporation. Red and green circles represent the spots identified by EDS as KCl and NaCl, respectively.

The KCl-seed crystal was also analyzed using SEM-EDS (Figure 6C). Most crystals on the surface of the KCl-seed are NaCl. The KCl core of the seed could not be detected with EDS, as the excrescences grown on top of it significantly hinder a clear signal from the engulfed crystal. There are at least two sets of crystals in clear epitaxial relation: the grown KCl seed, mostly covered by NaCl crystals, and the set on the left, diagonally oriented regarding the seed but with parallel edges of NaCl and KCl. Besides, KCl crystals

developed on the surface of the epitaxially grown NaCl crystal, evidencing epitaxy of both compounds: NaCl on KCl and KCl on NaCl. These epitaxially grown KCl and NaCl crystals engulfed the KCl seed. Most often, the epitaxially grown crystals followed the crystallographic orientation of the substrate.

In a rough approximation, one can use the lattice constants to evaluate such mismatch (unit cell parameters are linear—1D—and epitaxial match or mismatch is 2D, thus, this comparison should not be straightforward). Both NaCl and KCl belong to the cubic crystal system, displaying only one lattice constant, respectively, a = 5.64010 Å and 6.28790 Å [37], as shown in Figure 7. Hence, the mismatch < 15% is compatible with epitaxial growth in this system. Even so, formation of a thin stressed growth layer of KCl over NaCl is also visible, consistent with the Stranski–Krastanov mechanism [12,27,38]. Moreover, 2D lattice matching estimations showed that no characteristic match could be observed between any of the pairs of crystals used in this study. Most of the calculated non-dimensional potential energy values are approximately 1, indicating incommensurism [21]. Detailed lattice matching calculations can be found on the Supplementary Information.

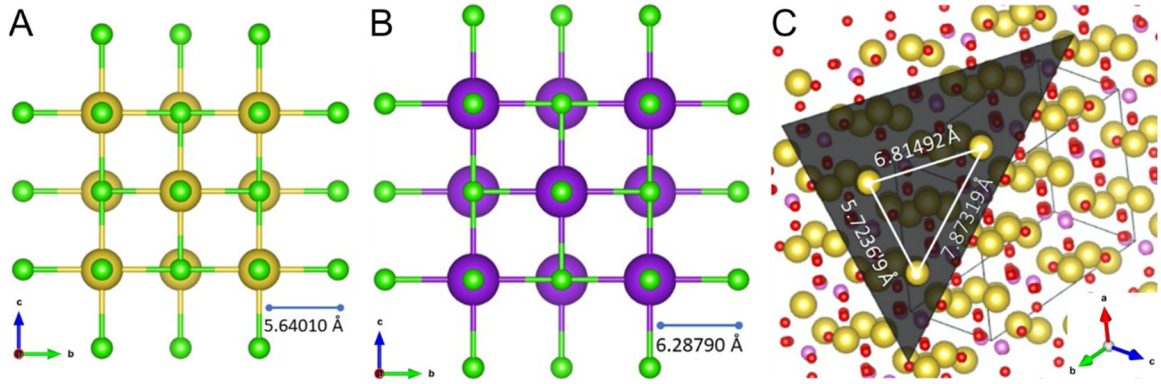

Figure 7. Projection of (100) planes of (**A**) NaCl, (**B**) KCl, and (**C**) plane (111) of Na_2SO_4 with Na depicted in yellow, K in purple, Cl in green, S in pink and O in red. Lattice parameters taken considering room temperature and pressure [37]. Projections made with VESTA software [39].

In our previous work, we have also observed epitaxial growth in the NaCl–KCl pair [4,5] during 0.5 L scale batchwise seeded evaporative crystallization from boiling solutions at approximately 110 °C. However, in those experiments, epitaxial growth of KCl on NaCl seeds was more abundant than vice-versa, in disagreement with the droplet crystallization experiments. In the present study, epitaxial NaCl crystals have covered the KCl substrate surface almost completely, unlike KCl deposits upon a NaCl substrate. Besides, these excrescences were seen in much higher proportions when compared to the analogue experiment seeded with NaCl. This inversion on the 'epitaxy preference' follows an inversion on the solubility of the salts due to the change in temperature. The salt with the higher solubility is observed to show preferential epitaxial growth in relation to the less soluble salt in both cases (25 °C—NaCl 5.24 mol·kg^{-1}, KCl 1.95 mol·kg^{-1}; 110 °C—NaCl 4.64 mol·kg^{-1}, KCl 4.85 mol·kg^{-1}). This is probably the case, as due to higher residual supersaturation, in the presence of a foreign surface, heterogeneous nucleation on the substrate seed is more likely to occur.

It is also possible that the surface roughness of the parent crystal also plays a role in controlling epitaxial growth. A rough surface contains more kinks and steps, which are known to ease heterogeneous nucleation. Here, under simultaneous NaCl and KCl crystallization, the NaCl crystal surface is smooth, whereas the KCl surface is rough. Hence, this explains why NaCl is a poorer substrate for epitaxial growth than KCl and why seeding with KCl lead to the large extent of particle engulfment by the NaCl excrescences. Mithen and Sear [40] also reported crystallization on crystalline surfaces to be largely influenced by the surface features, e.g., geometry and the intermolecular interactions

between surface and nucleus. This also explains the higher number of crystals nucleating earlier around the seed-crystal when NaCl was seeded, in comparison to KCl-seeded experiments. As less supersaturation is getting consumed on growth/epitaxial growth on the seed, heterogeneous nucleation is induced elsewhere.

3.2. NaCl–Na_2SO_4–H_2O System

In the NaCl–Na_2SO_4–H_2O droplet under evaporation, the NaCl seed crystal presented a slight dissolution at the first minutes of the experiment, but after 14 min of evaporation, it started to grow (Figure 8). The edges, rounded by dissolution, healed and the typical hopper habit started to develop. The corners overgrowth of the NaCl seed crystal is easily visible at 26 min. After 40 min of evaporation, tiny crystals appeared all over the droplet (glass-droplet interface), growing to sizes up to 50 microns. Interestingly, none of the newly formed crystals were formed in the NaCl seed surface. Photomicrographs of the droplet after 61 and 63 min were taken with crossed polarizers and a gypsum plate to highlight the differences between the two compounds. Crystalline sodium sulphate may crystallize as the anhydrous salt (thenardite, orthorhombic crystal system) or the decahydrate form ($Na_2SO_4 \cdot 10H_2O$, mirabilite, monoclinic). Both forms are birefringent and produce interference colors under crossed polarizers. Crystalline NaCl, on the other hand, belongs to the cubic system and is isotropic to light and does not produce interference colors under crossed polarizers.

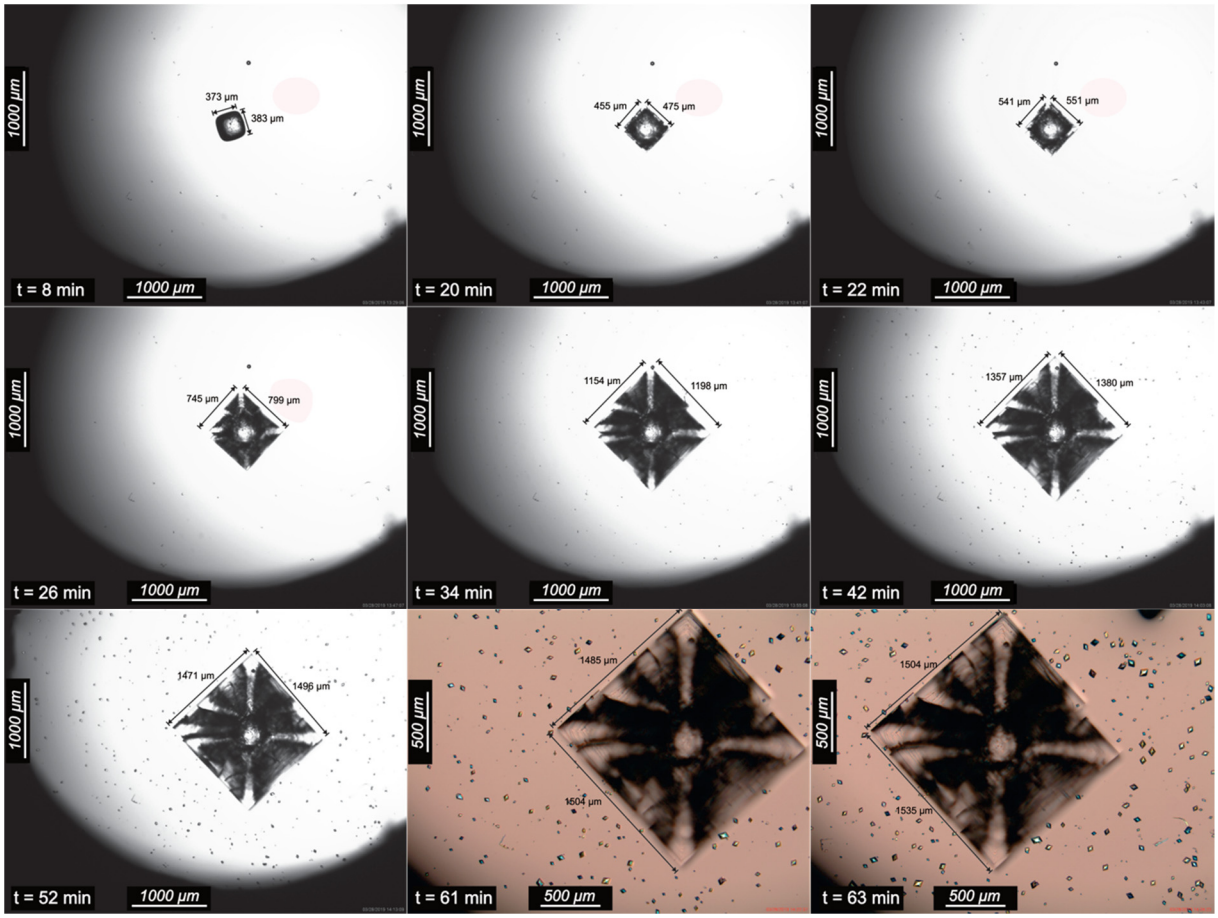

Figure 8. Optical photomicrographs along time of the NaCl–Na_2SO_4–H_2O droplet under evaporation seeded with NaCl.

According to the phase diagram (Figure 1), under the concentration and temperature used in the experiments, the anhydrous salt Na_2SO_4 (thenardite) is the stable form. The bipyramidal habit observed in the experiments is also characteristic of thenardite. It is

noteworthy that, in a Na_2SO_4-H_2O solution, the formation of thenardite is not expected below 32.4 °C, unless relative humidity is under 71% [41].

In situ photomicrographs of a single Na_2SO_4 seed crystal in a droplet of the NaCl–Na_2SO_4–H_2O system are presented in Figure 9. The Na_2SO_4 seed crystal was abraded during the first 10 min, and, after that, crystal growth took place and crystal edges were reconstructed, so what appears to be a top view of a typical bipyramidal habit developed. After approximately 35 min of evaporation, two NaCl crystals nucleated on adjacent faces of the pre-existent Na_2SO_4 crystal and grew crystallographically aligned with the parent crystal whilst tiny Na_2SO_4 crystals appeared all over the droplet (highlighted by the gypsum plate at t = 58 min). Two minutes later, a new NaCl crystal appeared on the surface of a primarily nucleated Na_2SO_4 crystal, in the vicinity of the seed. Growth of NaCl crystals continued until they reached the same size of the Na_2SO_4 seed crystal, while the newly formed Na_2SO_4 crystals showed a much less growth. This is expected as Na_2SO_4 solubility at the eutonic condition is almost ten times lower than the solubility of NaCl (Figure 1), thus the net yield of Na_2SO_4 is also almost ten times lower. Moreover, the growth of the sulphate seed was probably also hindered by the deposited NaCl crystals on its surface, which might have led to the increase of the Na_2SO_4 supersaturation and to the observed Na_2SO_4 nucleation event. It is likely that, given enough time, the epitaxial NaCl crystals would completely engulf the seeded Na_2SO_4 crystal. NaCl crystals displayed hopper habit, visible in the two 'epitaxial' NaCl crystals and the other crystal at 38 min (Figure 9). Furthermore, underdeveloped crystalline faces can be observed on the NaCl deposits on the seed facing the NaCl deposit on the newly nucleated sodium sulphate, most likely due to a depletion of available ions for crystal growth.

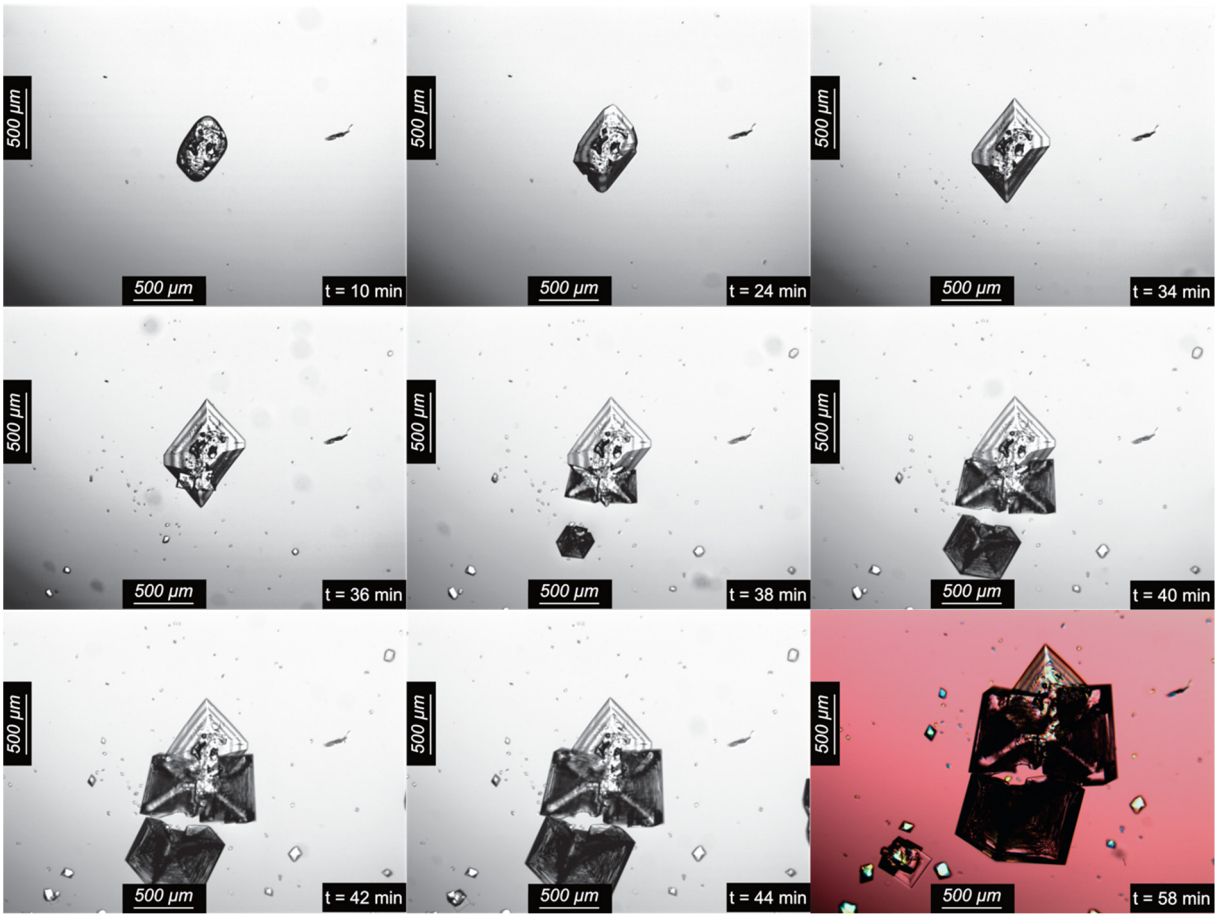

Figure 9. Optical photomicrographs along time of the NaCl–Na_2SO_4–H_2O droplet under evaporation seeded with Na_2SO_4.

SEM images of the experiment with NaCl seed crystals are shown in Figure 10A. Seed surface is smooth, except for the few bipyramidal sodium sulphate crystals on its surface (Figure 10B). These deposited crystals were not as numerous as the ones seen nucleating in solution, yet they were found in matching sizes (up to 100 µm). A hopper cavity formed during NaCl growth (Figure 10C) is visible due to a breakage on the layer of crystalline material that formed over that cavity. This closed hopper cavity emphasizes the possibility of generation of fluid inclusions under these conditions. Fluid inclusions are not desired characteristics on products, as they lower purity when entailing a compound other than the crystal composition.

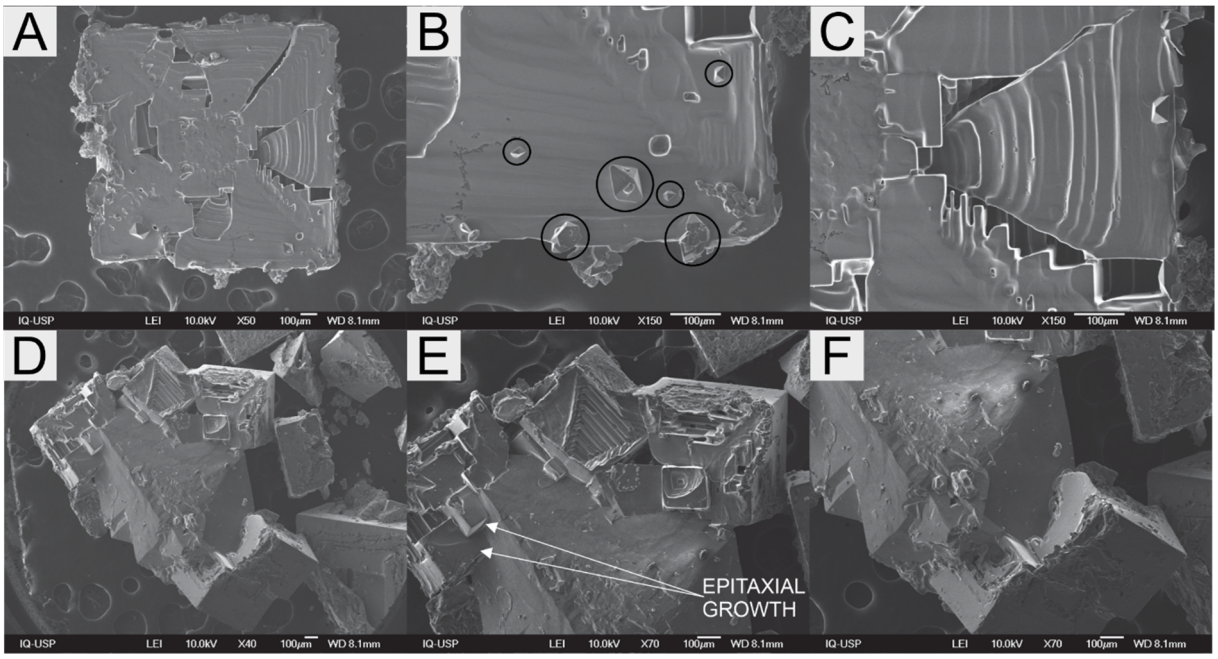

Figure 10. SEM image of (**A**) the NaCl seed grown after 63 min on the NaCl–Na_2SO_4–H_2O droplet under evaporation; (**B**) Na_2SO_4 crystals on the seed surface; (**C**) a hopper cavity of the seed crystal; (**D**) Na_2SO_4 seed grown after 58 min on the NaCl–Na_2SO_4–H_2O droplet under evaporation; (**E**,**F**) epitaxial formations of NaCl crystals on top of the Na_2SO_4 seed.

SEM image on Figure 10D shows the Na_2SO_4 grown seed. Flat surfaces observed here are consistent with the fringes seen in polarized light, indicating a uniform variation in Na_2SO_4 crystal thickness. Figure 10E, F focuses on the epitaxial growth of NaCl crystals on (111) plane at the Na_2SO_4 substrate. Hopper habit is clearly visible in all NaCl crystals. However, it is uncertain whether these epitaxial formations are oriented or non-oriented epitaxial crystals.

Epitaxial deposits without crystallographic orientation with respect to the seed crystal, were seen in both the NaCl–KCl–H_2O and NaCl–Na_2SO_4–H_2O systems. This is compatible with the 3D island growth mechanism proposed by Stranski–Krastanov [12,38], which is expected for a mismatch between the crystal lattice constants of 15% or less [42,43]. NaCl is seen to grown on the (111) face of Na_2SO_4 (thenardite), which belongs to the orthorhombic crystal system. Hence, the lattice mismatch can be evaluated considering the interatomic distances between the atoms on this face (Figure 7C), as there seems to be higher coherence between NaCl (100) face and Na_2SO_4 (111) face. However, when comparing lattice parameter pairs, only one of the thenardite constants (a = 5.7236 Å) differ (slightly) from the NaCl's constant. In their study on epitaxy-nucleated crystals over crystalline surfaces, Mithen and Sear [24] report that oriented epitaxy relies on the coherence of the lattice parameters, i.e., crystal lattices of the nucleus and the substrate closely match. Yet, epitaxial formations were still seen in this study—although not oriented—despite poor matching between most of the lattice parameters. On the other hand, this observation

agrees with Pashley's [18] reports for epitaxial thin film surfaces that the low misfit value, although significant under certain conditions, is not an essential criterion for epitaxial growth. Sarma et al. [44] studied the crystallization of several pairs of organic compounds over different inorganic crystals with well-defined crystallographic planes and found little correlation between lattice matching, epitaxy and preferred nucleation orientation. They concluded that when it comes to epitaxy, multiple mechanisms take place and that intermolecular forces as well as growth anisotropy also play a role.

Similar to NaCl–KCl–H_2O system, here the epitaxial growth of NaCl upon Na_2SO_4 is observed in large proportions than the inverse. Additionally, in the NaCl–Na_2SO_4–H_2O system, the salt with the higher solubility showed preference for epitaxial growth in relation to the less soluble salt (25 °C—NaCl 5.74 mol·kg^{-1}, Na_2SO_4 0.74 mol·kg^{-1}). This result corroborates with previous analysis of the NaCl–KCl–H_2O system regarding the higher residual supersaturation for the unseeded salt with higher solubility. It is likely that this eases the overcoming of the energy barrier for nucleation of the epitaxial crystal on the surface of the parent crystal. In the conditions studied here, some of the non-seed crystals yielded primarily nucleated single crystals in solution, instead of developing epitaxial relations with the seed. This suggests that the energy barrier for nucleation upon heterogeneous impurities in solution is at least equal to, if not lower, than the analogous barrier for nucleation upon the surface of the seed.

Furthermore, on NaCl–KCl–H_2O system, surface roughness could be somewhat associated with epitaxial growth. Here, the NaCl–Na_2SO_4–H_2O system partially follows this 'rule', as NaCl grows upon the Na_2SO_4 surfaces up to sizes comparable to the seeded crystal, whereas just tiny sparse Na_2SO_4 appear on the flat NaCl substrate surface along with several other idiomorphic bipyramidal Na_2SO_4 crystals. Na_2SO_4 seed surfaces are not visibly rough but given its initial abraded state, a higher roughness, when compared to the NaCl seed, is expected.

In the NaCl–Na_2SO_4–H_2O system, the NaCl hopper habit also prevails. In evaporative crystallization in a droplet, crystal growth removes ions from the solution, which are only partially replenished in the growth layer of the crystal by natural convection, so the ion availability decreases [32,45]. As the consumption of SO_4^{-2} ions is much lower than the other ions—due to the lower driving force, i.e., supersaturation, for sodium sulphate formation—the accumulation of SO_4^{-2} ions around the growing layer may sterically hamper NaCl growth by hindering growth units to reach the surface. Consequently, the growth process becomes partially limited by diffusion. As diffusion is more effective in the vicinity of the edges and corners of the crystal, these regions grow faster than the centers of the faces, giving rise to the hopper habit. For the NaCl–Na_2SO_4–H_2O and NaCl–KCl–H_2O systems, both crystallizing salts require a common ion (Na^+ and Cl^-, respectively). That not only causes competition for the common ion but also promotes a sharper decrease of the available ions.

3.3. NaCl–$CaSO_4$–H_2O System

Images of the eutonic solution of the NaCl–$CaSO_4$–H_2O system seeded with a single NaCl crystal are presented in Figure 11. In the first 10 min of evaporation, the seed crystal did grow slightly, and its edges were healed, i.e., rounded edges became flat. From 10 min on, NaCl growing seed is seen to develop hopper habit. Up to 60 min, overgrown edges are seen to increase and reach each other, forming a cavity in the center of the face of the cubic crystal, which remained open.

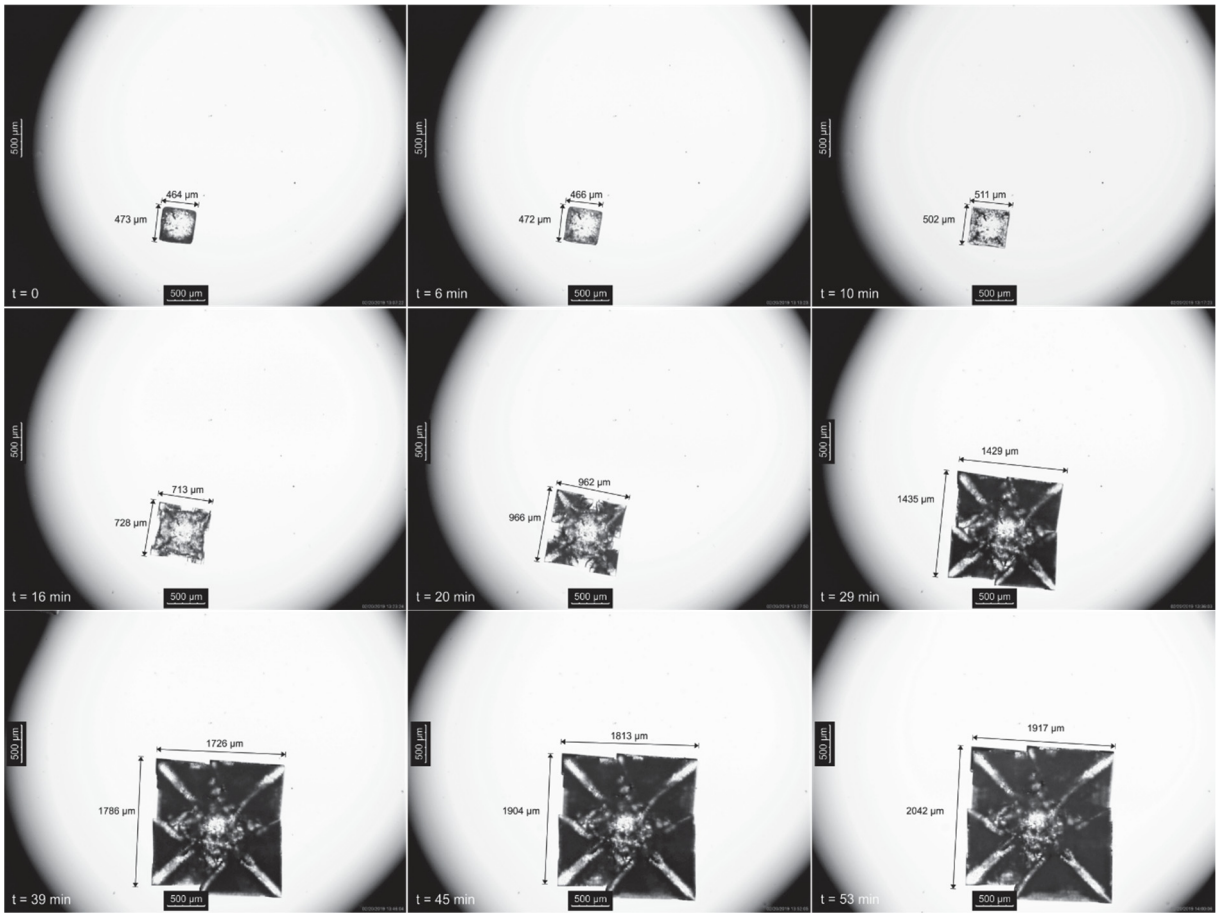

Figure 11. Optical photomicrographs along time of the NaCl–$CaSO_4$–H_2O droplet under evaporation seeded with NaCl.

Even though during evaporation the solution became supersaturated with respect to anhydrous $CaSO_4$, which crystallized, calcium sulphate crystals are not visible through optical microscopy. SEM-EDS image displays the NaCl seed (Figure 12A); its face central cavities can be clearly observed, as well as a step-like-structure, comprising the inner (hollow) walls of the cavity. Two of the edges are seen broken because, due to hopper growth, edges are thin and fragile. Calcium sulphate in solution was reported to interfere with the growth of NaCl by Zago et al. [4,7]. In their work, evaporation was performed at 110 °C and hopper growth was also observed, as well as more prominent fluid inclusions in the product. $CaSO_4$ was also related to increased roughness on NaCl crystal surfaces.

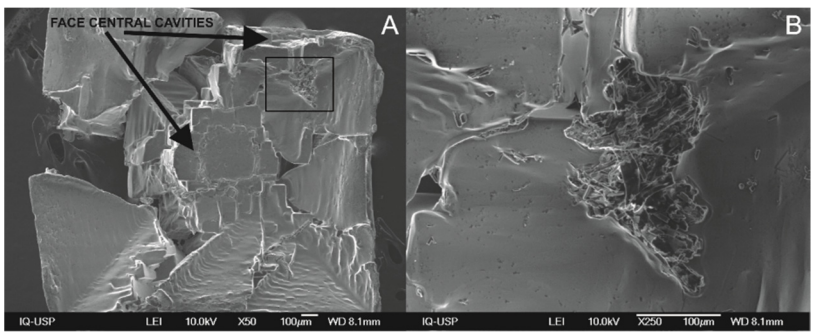

Figure 12. SEM image of (**A**) NaCl seed grown after 60 min on the NaCl–$CaSO_4$–H_2O droplet under evaporation and (**B**) $CaSO_4$ on the surface of the grown seed (square on A indicates the enlarged area shown on (**B**)).

Figure 12B reveals shapeless deposits of $CaSO_4$ on the surface of the NaCl parent crystal. Tiny $CaSO_4$ crystals seen are xenomorphic or anhedral, as their shape is determined by the surrounding crystals [46]. No isolated $CaSO_4$ single crystals were seen. Some elongated/needle-like crystals, which can be $CaSO_4$, are seen partially buried on the NaCl surface, likely due to the higher NaCl growth rate compared to $CaSO_4$ that ends up in particle engulfment. This is not completely unexpected, as the solubility of NaCl is approximately 150 times higher than $CaSO_4$ solubility. Thus, the much larger amount of crystallized NaCl can easily grow a layer over tiny calcium sulphate crystals, burying them on the crystalline structure. Moreover, despite the thermodynamic predictions of $CaSO_4$ crystallization as anhydrite, its low kinetics [47] plus concentration fluctuations and local supersaturation conditions—due to natural convection only—may lead to the formation of other $CaSO_4$ phases, such as gypsum. The formation of amorphous phases and hemihydrate ($CaSO_4 \cdot 0.5H_2O$) as intermediates in the precipitation of gypsum has been reported elsewhere [48,49].

Overall, previous studies reported in the literature mention only lattice matching and recently intermolecular interactions and surface geometry as criteria for epitaxial growth [12,24,40,44]. However, in all previous studies, a single compound was nucleating and growing on top of an inert crystalline substrate. For this reason, relative solubilities between the crystallizing compounds were not a parameter. Here, it is observed that a higher proportion of epitaxial growth on the surface of the seeded crystal occurs when the most soluble compound is not seeded, e.g., NaCl on KCl, when KCl was seeded and NaCl on Na_2SO_4 when Na_2SO_4 was seeded. The solubility ratios for NaCl regarding KCl, Na_2SO_4 and $CaSO_4$ are, respectively, 2.7:1, 7.8:1 and 152:1. Although $CaSO_4$ was not seeded here, evidence of its seeds serving as nuclei for the formation of NaCl seeds were found in previous studies [7].

4. Conclusions

Epitaxial growth develops both in the aqueous NaCl–KCl and the aqueous NaCl–Na_2SO_4 systems, with NaCl growth upon the other substrates being more prominent than the inverse. Larger amounts of NaCl nucleated on seed crystals of KCl and Na_2SO_4 is related to the higher solubility of NaCl compared to the seeded compounds. On NaCl seed crystals, mostly tiny KCl, Na_2SO_4 and xenomorphic Ca_2SO_4 deposits were observed.

Epitaxial deposits develop both with and without crystallographic alignment with the parent crystal. This feature and the crystallographic mismatch between the crystalline lattices of the parent and the epitaxial crystal are consistent with the Stranski–Krastanov 3D growth mechanism. Epitaxial growth leads to multicomponent particles, which hampers downstream separation of the solids. Seed crystals may be covered in large extent by the epitaxial crystals, a condition that reduces the surface area of the seed and affects supersaturation control in industrial crystallizers. Formation of hopper habit in NaCl favors formation of fluid inclusions which reduces purity and affects downstream handling of the crystals.

Understanding how crystals interact during simultaneous crystallization is of importance when performing crystallization from multicomponent complex solutions. Beyond choosing the most adequate seeds, the order in which solutes crystallize might aid in the control of particle morphologies and enhance final purity.

Supplementary Materials: The following are available online at https://www.mdpi.com/article/10.3390/cryst11091122/s1, Figure S1: Optical photomicrographs along time of the NaCl–H_2O droplet under evaporation seeded with NaCl; Figures S2–S4: 2D Lattice matching calculations.

Author Contributions: The manuscript was written through contributions of all authors. Conceptualization, F.M.P., P.F.M.J. and G.P.Z.; methodology, F.M.P. and A.S.L.; software, F.M.P (OLI Studio), F.R.D.A. (VESTA); formal analysis, F.M.P. and F.R.D.A.; investigation, F.M.P.; writing—original draft preparation, F.M.P.; writing—review and editing, F.M.P., F.R.D.A., G.P.Z., A.S.L. and M.M.S.; supervision, M.M.S.; project administration, F.M.P.; funding acquisition, F.M.P. and M.M.S. All authors have read and agreed to the published version of the manuscript.

Funding: The financial support of the Coordination for the Improvement of Higher Education Personnel (CAPES, PNPD, File number 88882.315573/2019-01) is gratefully acknowledged.

Acknowledgments: F.M.P. heartfully acknowledges Denise Trigilio Tavares for administrative, technical, and, most of all, emotional support.

Conflicts of Interest: The authors declare no conflict of interest.

References

1. Lewis, A.; Seckler, M.; Kramer, H.; van Rosmalen, G. *Industrial Crystallization: Fundamentals and Applications*; Cambridge University Press: Cambridge, UK, 2015.
2. Plumb, K. Continuous Processing in the Pharmaceutical Industry: Changing the Mind Set. *Chem. Eng. Res. Des.* **2005**, *83*, 730–738. [CrossRef]
3. Matsuoka, M.; Yamamoto, K.; Uchida, H.; Takiyama, H. Crystallization phenomena in ternary systems: Nucleation of KCl during dissolution of NaCl. *J. Cryst. Growth* **2002**, *244*, 95–101. [CrossRef]
4. Penha, F.M.; Zago, G.P.; Seckler, M.M. Strategies To Control Product Characteristics in Simultaneous Crystallization of NaCl and KCl from Aqueous Solution: Seeding with KCl. *Cryst. Growth Des.* **2019**, *19*, 1257–1267. [CrossRef]
5. Penha, F.M.; Zago, G.P.; Nariyoshi, Y.N.; Bernardo, A.; Seckler, M.M. Simultaneous Crystallization of NaCl and KCl from Aqueous Solution: Elementary Phenomena and Product Characterization. *Cryst. Growth Des.* **2018**, *18*, 1645–1656. [CrossRef]
6. Zago, G.P.; Penha, F.M.; Seckler, M.M. Product characteristics in simultaneous crystallization of NaCl and CaSO 4 from aqueous solution under different evaporation rates. *Desalination* **2019**, *457*, 85–95. [CrossRef]
7. Zago, G.P.; Penha, F.M.; Seckler, M.M. Product characteristics in simultaneous crystallization of NaCl and CaSO4 from aqueous solution with seeding. *Desalination* **2020**, *474*, 114180. [CrossRef]
8. Chambers, S.A. Epitaxial growth and properties of thin film oxides. *Surf. Sci. Rep.* **2000**, *39*, 105–180. [CrossRef]
9. Brune, H. Epitaxial Growth of Thin Films. *Surf. Interface Sci.* **2014**, *4*, 421–477. [CrossRef]
10. Kelso, M.V.; Mahenderkar, N.K.; Chen, Q.; Tubbesing, J.Z.; Switzer, J.A. Spin Coating Epitaxial Films. *Science* **2019**, *364*, 166–169.
11. Markov, I.V. *Crystal Growth for Beginners: Fundamentals of Nucleation, Crystal Growth and Epitaxy*; World Scientific: Singapore, 2003.
12. Glikin, A.E. *Polymineral- Metasomatic Crystallogenesis*; Springer: Berlin/Heidelberg, Germany, 2009.
13. Chernov, A.A. Nucleation and Epitaxy. In *Modern Crystallography III: Crystal Growth*; Springer: Berlin/Heidelberg, Germany, 1984; pp. 48–103.
14. Shtukenberg, A.G.; Astilleros, J.M.; Putnis, A. Nanoscale observations of the epitaxial growth of hashemite on barite (0 0 1). *Surf. Sci.* **2005**, *590*, 212–223. [CrossRef]
15. Niekawa, N.; Kitamura, M. Role of epitaxy-mediated transformation in Ostwald's step rule: A theoretical study. *CrystEngComm* **2013**, *15*, 6932–6941. [CrossRef]
16. Croker, D.; Hodnett, B.K. Mechanistic Features of Polymorphic Transformations: The Role of Surfaces. *Cryst. Growth Des.* **2010**, *10*, 2808–2816. [CrossRef]
17. Royer, L. Recherches experimentalles sur l'epitaxie on orientation mutuelle des cristaux des espices differentes. *Bull. Soc. Fr. Miner.* **1928**, *55*, 77–159.
18. Pashley, D.W. The study of epitaxy in thin surface films. *Adv. Phys.* **1956**, *5*, 173–240. [CrossRef]
19. Pashley, D.W. The nucleation, growth, structure and epitaxy of thin surface films. *Adv. Phys.* **1965**, *14*, 327–416. [CrossRef]
20. Van der Merwe, J.H. Misfitting monolayers and oriented overgrowth. *Discuss. Faraday Soc.* **1949**, *5*, 201–214. [CrossRef]
21. Hillier, A.C.; Ward, M.D. Epitaxial interactions between molecular overlayers and ordered substrates. *Phys. Rev. B Condens. Matter Mater. Phys.* **1996**, *54*, 14037–14051. [CrossRef] [PubMed]
22. Mitchell, C.A.; Yu, L.; Ward, M.D. Selective nucleation and discovery of organic polymorphs through epitaxy with single crystal substrates. *J. Am. Chem. Soc.* **2001**, *123*, 10830–10839. [CrossRef] [PubMed]
23. Turnbull, D.; Vonnegut, B. Nucleation Catalysis. *Ind. Eng. Chem.* **1952**, *44*, 1292–1298. [CrossRef]
24. Mithen, J.P.; Sear, R.P. Epitaxial nucleation of a crystal on a crystalline surface. *Eur. Lett.* **2014**, *1105*, 8004. [CrossRef]
25. Mutaftschiev, B. *The Atomistic Nature of Crystal Growth*; Springer: Berlin/Heidelberg, Germany, 2013.
26. Springholz, G.; Frank, N.; Bauer, G. The origin of surface roughening in lattice-mismatched Frank van der Merwe type heteroepitaxy. *Thin Solid Films* **1995**, *267*, 15–23. [CrossRef]
27. Baskaran, A.; Smereka, P. Mechanisms of Stranski-Krastanov growth. *J. Appl. Phys.* **2012**, *111*, 044321. [CrossRef]
28. Blijlevens, M.R.; Townsend, E.R.; van Enckevort, W.J.P.; Meijer, J.A.M.; Vlieg, E. Additive induced pseudo-homoepitaxy of nanoneedles on NaCl crystals. *J. Cryst. Growth* **2018**, *498*, 43–50. [CrossRef]
29. Pashley, D.W. Epitaxy growth mechanisms. *Mater. Sci. Technol.* **1999**, *15*, 2–8. [CrossRef]
30. Becheleni, E.; Borba, R.; Seckler, M.; Rocha, S. Water recovery from saline streams produced by electrodialysis. *Environ. Technol.* **2015**, *36*, 386–394. [CrossRef]
31. Selzer, D.; Frank, C.; Kind, M. On the effect of the continuous phase on primary crystal nucleation of aqueous KNO_3 solution droplets. *J. Cryst. Growth* **2019**, *517*, 39–47. [CrossRef]
32. Desarnaud, J.; Derluyn, H.; Carmeliet, J.; Bonn, D.; Shahidzadeh, N. Hopper Growth of Salt Crystals. *J. Phys. Chem. Lett.* **2018**, *9*, 2961–2966. [CrossRef]

33. Desarnaud, J.; Derluyn, H.; Carmeliet, J.; Bonn, D.; Shahidzadeh, N. Nucleation and growth of sodium chloride in confined geometries. In Proceedings of the SWBSS 2014, 3rd International Conference on Salt Weathering of Buildings and Stone Sculptures, Brussels, Belgium, 14–16 October 2014; pp. 17–33.
34. Tsukamoto, K. In-situ observation of crystal growth and the mechanism. *Prog. Cryst. Growth Charact. Mater.* **2016**, *62*, 111–125. [CrossRef]
35. Bakker, R.J. Package FLUIDS. Part 4: Thermodynamic modelling and purely empirical equations for H2O-NaCl-KCl solutions. *Mineral. Petrol.* **2012**, *105*, 1–29. [CrossRef]
36. Priya, M.; Mahadevan, C.K. Studies on multiphased mixed crystals of NaCl, KCl and KI. *Cryst. Res. Technol.* **2009**, *44*, 92–102. [CrossRef]
37. Walker, D.; Verma, P.K.; Cranswick, L.M.; Jones, R.L.; Clark, S.M.; Buhre, S. Halite-sylvite thermoelasticity. *Am. Mineral.* **2004**, *89*, 204–210. [CrossRef]
38. Prieto, J.E.; Markov, I. Stranski-Krastanov mechanism of growth and the effect of misfit sign on quantum dots nucleation. *Surf. Sci.* **2017**, *664*, 172–184. [CrossRef]
39. Momma, K.; Izumi, F. VESTA 3 for three-dimensional visualization of crystal, volumetric and morphology data. *J. Appl. Crystallogr.* **2011**, *44*, 1272–1276. [CrossRef]
40. Mithen, J.P.; Sear, R.P. Computer simulation of epitaxial nucleation of a crystal on a crystalline surface. *J. Chem. Phys.* **2014**, *140*, 084504. [CrossRef]
41. Rodriguez-Navarro, C.; Doehne, E.; Sebastian, E. How does sodium sulfate crystallize? Implications for the decay and testing of building materials. *Cem. Concr. Res.* **2000**, *30*, 1527–1534. [CrossRef]
42. Glikin, A.; Plotkina, J. Disorientation Effects of Epitaxy At Aqueous Media. *Mater. Struct.* **1999**, *6*, 155–158.
43. Ruiz-Agudo, E.; Putnis, C.V.; Putnis, A. Coupled dissolution and precipitation at mineral–fluid interfaces. *Chem. Geol.* **2014**, *383*, 132–146. [CrossRef]
44. Sarma, K.R.; Shlichta, P.J.; Wilcox, W.R.; Lefever, R.A. Epitaxy versus oriented heterogeneous nucleation of organic crystals on ionic substrates. *J. Cryst. Growth* **1997**, *174*, 487–494. [CrossRef]
45. Zhang, J.; Zhang, S.; Wang, Z.; Zhang, Z.; Wang, S.; Wang, S. Hopper-like single crystals of sodium chloride grown at the interface of metastable water droplets. *Angew. Chem. Int. Ed.* **2011**, *50*, 6044–6047. [CrossRef] [PubMed]
46. Fay, A.H. *A Glossary of the Mining and Mineral Industry*; U.S. Government Printing Office: Washington, DC, USA, 1920.
47. Freyer, D.; Voigt, W. Crystallization and Phase Stability of CaSO4and CaSO4- Based Salts. *Mon. Chem.* **2003**, *134*, 693–719. [CrossRef]
48. Wang, Y.W.; Kim, Y.Y.; Christenson, H.K.; Meldrum, F.C. A new precipitation pathway for calcium sulfate dihydrate (gypsum) via amorphous and hemihydrate intermediates. *Chem. Commun.* **2012**, *48*, 504–506. [CrossRef]
49. Van Driessche, A.E.; Benning, L.G.; Rodriguez-Blanco, J.D.; Ossorio, M.; Bots, P.; García-Ruiz, J.M. The Role and Implications of Bassanite as a Stable Precursor Phase to Gypsum Precipitation. *Science* **2012**, *336*, 69–72. [CrossRef]